

The yielding transition in amorphous solids under oscillatory shear deformation

Premkumar Leishangthem,¹ Anshul D. S. Parmar,^{1,2} and Srikanth Sastry¹

¹*Jawaharlal Nehru Center for Advanced Scientific Research, Jakkur Campus, Bengaluru 560064, India*

²*TIFR Center for Interdisciplinary Sciences, 21 Brundavan Colony, Narsingi, Hyderabad 500075, India*

Amorphous solids are ubiquitous among natural and man-made materials. Often used as structural materials for their attractive mechanical properties, their utility depends critically on their response to applied stresses. Processes underlying such mechanical response, and in particular the yielding behaviour of amorphous solids, are not satisfactorily understood. Although studied extensively [1–14], observed yielding behaviour can be gradual and depend significantly on conditions of study, making it difficult to convincingly validate existing theoretical descriptions of a sharp yielding transition [4, 6, 8, 13, 15]. Here, we employ oscillatory deformation as a reliable probe of the yielding transition. Through extensive computer simulations for a wide range of system sizes, we demonstrate that cyclically deformed model glasses exhibit a sharply defined yielding transition with characteristics that are independent of preparation history. In contrast to prevailing expectations [4, 8, 12], the statistics of avalanches reveals no signature of the impending transition, but exhibit dramatic, qualitative, changes in character across the transition.

The mechanical response to applied stresses or deformation is a basic material characteristic of solids, both crystalline and amorphous. Whereas the response to small perturbations are described by elastic moduli, the *plastic*, irreversible, response to large deformation is often more important to characterise, as it determines many material parameters such as strength and ductility, and is also of relevance to thermomechanical processing of metallic glasses [16]. Amorphous solids lack the translational symmetry of crystals, and thus no obvious analogs to dislocation defects in terms of which plasticity in crystals has been sought to be understood. Based on work over the last decades, it is appreciated that plasticity arises in amorphous solids through spatially localized reorganisations [1, 2, 17], termed shear transformation zones, and that such localized zones interact with each other through long ranged elastic strains they induce [18]. While many details of the nature of these localized regions of *non-affine* displacements remain to be worked out, they form the basis of analyses and models of *elasto-plasticity* and yielding [6, 13, 18–20]. Many analyses have employed computer simulations of atomistic models of glasses, aiming to elucidate key features of plastic response [1–3] on atomic scales. While several studies have been conducted at finite shear rates (*e.g.* [11, 13]), many studies have focussed on behaviour in the athermal, quasi-static (AQS) [3, 5, 6, 14, 21] limit, wherein the model glasses studied remain in zero temperature, local energy minimum, configurations as they are sheared quasi-statically. Such deformation induces discontinuous drops in energy and stress with corresponding nonaffine displacements that are highly spatially correlated, and exhibit power law distributions in size. In analogy with similar *avalanches* that arise in diverse context of intermittent response in disordered systems, from earthquakes, crackling noise in magnetic systems, depinning of interfaces in a disordered medium *etc.* [22], a theoretical description of yielding in amorphous solids [4], predicts the mean avalanche size to diverge as the yielding transition is approached from below, leading to a

power law distribution with a diverging mean size at and above the transition. Indeed, it has been observed that (*e. g.* [5, 13, 21]) system spanning avalanches are present in the steady state beyond yield, whose sizes scale with system size. The character of avalanches upon approaching the yielding transition, however, has not received much attention, as also the differences between pre- and post-yield avalanches. Among the reasons is the sample to sample variability of behaviour below yield, in contrast with the universal behaviour seen in the post-yield regime. Here, we show that oscillatory deformation offers a robust approach to systematically probe behaviour above and below yielding. Oscillatory deformation is a widely used experimental technique as well as a common protocol in materials testing. However, barring some recent work [12, 23–25], it is not been employed widely to probe yielding in amorphous solids computationally. In the present work, we perform an extensive computational study of plastic response in a model glass former, over a wide range of system sizes, and amplitudes of deformation that straddle the yielding strain.

We study the Kob-Andersen 80:20 binary mixture Lennard-Jones glasses for a range of system sizes (see Methods for details). The glasses studied are prepared by performing a local energy minimization of equilibrated liquid configurations, at a reduced temperatures $T = 1$ and $T = 0.466$. The *inherent structures* so obtained represent poorly annealed ($T = 1$) and well annealed ($T = 0.466$) glasses. These glasses, referred to by the corresponding liquid temperature in what follows, are subjected to volume preserving shear deformation through the AQS protocol. The strain is incremented in the same direction in the case of *uniform strain*, whereas for oscillatory strain for a given maximum amplitude γ_{max} , a cycle of strain $0 \rightarrow \gamma_{max} \rightarrow 0 \rightarrow -\gamma_{max} \rightarrow 0$ is applied repeatedly over many cycles, till a steady state is reached. Results presented below, except Figure 1 (d) are from analysing steady state configurations. Further details concerning the simulations and analysis are presented in Methods and Supporting Information.

Stress and Energy across the Yielding Transition.- Previous work [23] has shown that as the amplitude of strain γ_{max} approaches a critical value γ_y from either side, the approach to the steady state becomes increasingly sluggish, with an apparent divergence at γ_y (see Supporting Information). We identify γ_y (~ 0.07) as the yield strain, as justified below. In Figure 1(a) we show the averaged stress-strain curves for $N = 4000$. For each γ_{max} , we obtain a maximum stress σ_{max} reached at $\gamma = \gamma_{max}$, which are plotted in Figure 1(b) for $T = 1, 0.466$, for $N = 4000, 32000$. Figure 1(b) also shows the stress-strain curves for the same cases obtained with uniform strain. Whereas stresses vary smoothly for uniform strain, with no sharp signature of the onset of yielding, and differ significantly for $T = 1$ and $T = 0.466$, they display a sharp, discontinuous, drop above $\gamma_{max} = 0.07$ (0.08 for $N = 4000$) for oscillatory strain. Interestingly, below γ_y , the maximum stress increases as a result of oscillatory deformation, indicative of hardening, consistently with previous results [26]. Above γ_y , repeated oscillatory deformation leads to a stress drop relative to values just below γ_y , indicating yielding. Figure 1 (c) displays the potential energies obtained over a full cycle in the steady state (see Supporting Information for evolution with cycles of strain). For $\gamma_{max} < \gamma_y$, the energies display a single minimum close to $\gamma = 0$, but above, bifurcate into two minima, indicating the emergence of plasticity. The stress-strain curves show a corresponding emergence of loops (Figure 1(a)) with finite area. Strain values at the minima for energy, γ_{Umin} and $\sigma_{xz} = 0$, γ_{σ_0} , are shown in Figure 1(d) as a function of the number of cycles for different γ_{max} . We note that $\gamma_{max} = 0.08$ displays interesting non-monotonic behaviour, with an initial decrease in these strain values, similar to smaller γ_{max} , but an eventual increase to larger strains, similar to the case $\gamma_{max} = 0.12$, in the yielded regime. Figure 1(e) shows γ_{Umin} and γ_{σ_0} vs. γ_{max} , which show an apparently continuous departure from nearly zero, signalling a transition at $\gamma_{max} \sim 0.07$. Figure 1(f) shows that the minimum energies in the steady state vs. γ_{max} decrease with increasing γ_{max} below γ_y , but increase above, reaching the same values for $T = 1$ and $T = 0.466$. These data demonstrate the presence of a sharp transition between a low strain regime where oscillatory shear produces better annealed, hardened, glasses to a yielded regime displaying stress relaxation and rejuvenation.

We next study (i) distribution of avalanche sizes, which we compute as the size of clusters of particles that undergo plastic rearrangements (see Methods for how they are identified), and (ii) distributions of the size of energy drops.

Distributions of Cluster Sizes.- In Figure 2 (a) we show the distributions $P(s)$ of avalanche sizes s for $N = 2000$, which display a characteristic power law decay with a cutoff. Although the cutoffs move to larger values as γ_{max} increases, we see no indication of a transition. To assess the role of system sizes, we compute the avalanche sizes for a variety of system sizes. Figure 2(b) shows the

avalanche size distribution for $N = 64000$. The distributions fall into two clear sets, corresponding to γ_{max} above and below γ_y . We compute and display in Figure 2 (c) the mean avalanche size $\langle s \rangle$ as a function of γ_{max} , for all studied system sizes. The striking observation is that below γ_y , $\langle s \rangle$ displays no system size dependence, and only a very mild dependence on γ_{max} , and no indication of the approach to γ_y . Above γ_y , a clear system size dependence is seen. Figure 2 (d) shows the same data vs. system size, revealing a roughly $N^{1/3}$ (or $\langle s \rangle \sim L$) dependence above γ_y , and minimal N dependence below. The $N^{1/3}$ dependence is consistent with previous results [5, 27] for mean energy drops, but the absence of system size dependence below, to our knowledge, has not been demonstrated before. We next ask whether the mean size of avalanches, for a given γ_{max} depend on the strain γ at which they appear, and conversely, for a given γ what the dependence on γ_{max} is. As shown in Figure 2 (e) ($N = 32000$, $T = 1$), for a given γ_{max} the γ dependence is weak and is the same for $\gamma_{max} < \gamma_y$ (and $\gamma_{max} > \gamma_y$), but the data fall into distinct groups for $\gamma_{max} < \gamma_y$ and $\gamma_{max} > \gamma_y$. The same pattern is seen for the full distributions (see Supporting Information). For a given γ_{max} , the avalanche distributions can be collapsed on to a master curve by scaling s by $\langle s \rangle$ (data not shown). The distributions of scaled sizes $\tilde{s} \equiv s / \langle s \rangle$, averaged over system size are shown in the inset of Figure 2 (f). The same data are shown, multiplied by $\tilde{s}^{3/2}$ in the main panel, and demonstrate that the character of the distributions are different above and below yield: whereas above γ_y one finds a range of sizes over which the power law form $P(s) \sim s^{-3/2}$ is clearly valid (and thus the cutoff arises purely because of system size), below γ_y this is not the case, and the qualitative shape of the distributions is different (with a cutoff function multiplying the power law) [4, 8, 12, 28].

Distributions of Energy Drops.- We now discuss the distributions of energy drops. Shown for $N = 4000$ and 32000 in Figures 3(a), and 3(b), these distributions show the same features as the avalanche sizes, but with a different power law exponent of ~ 1.25 (as found in [13]). Thus, the exponent depends on the quantity employed, and the avalanche size based on particle displacements is in closer agreement with mean field predictions). In Figure 3(c), we show the γ_{max} dependence of the mean energy drop, for different system sizes, which reveal the same pattern as the avalanche sizes, albeit with a stronger apparent size dependence below yield. However, the total energy drops for the whole system include also an elastic component, in addition to the plastic component. The component of the energy drop corresponding to the plastic regions alone, which are plotted in Figure 3 (d), to demonstrate that the plastic component has no system size dependence below yield. Figure 3 (e) shows the system size dependence of the mean energy drop (plastic component), and Figure 3 (f) shows the mean energy drop vs. γ for different γ_{max} ($N = 64000$, $T = 1$), revealing the same separation below and above yield as the avalanche

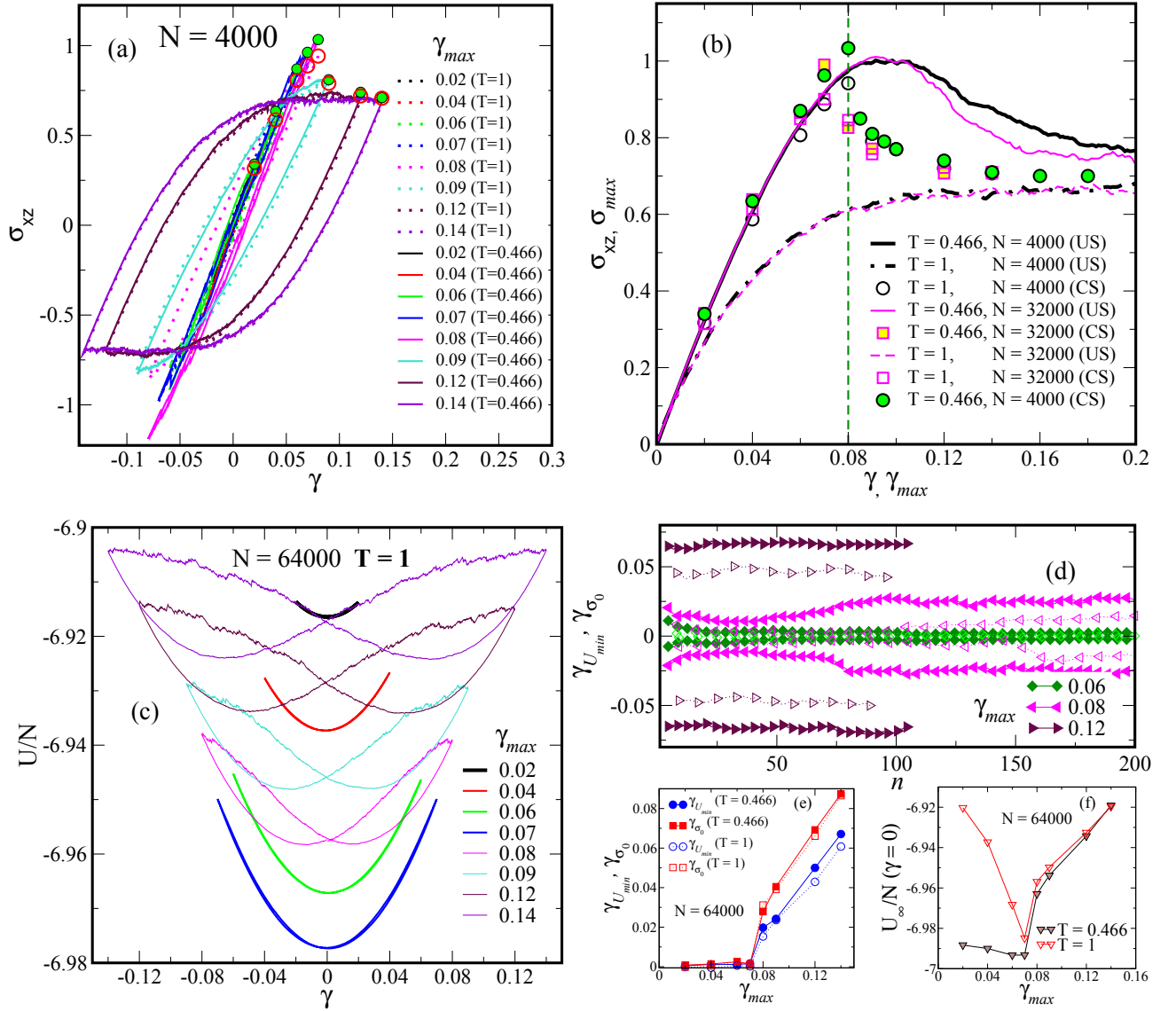


FIG. 1. Stress and energy across the yielding transition: (a) Stress-strain plots of the two differently annealed glasses for various strain amplitudes in the steady states of oscillatory shear deformation. Maximum stress in the cycle for each amplitude is marked by filled and open circles for $T = 0.466$ and $T = 1$ respectively. (b) Averaged stress-strain curves for uniform strain (US) are shown as lines - thick (black) for $N=4000$ and thin (magenta) for $N = 32000$ while solid and dashed lines represent $T=0.466$ and $T=1$ respectively. Maximum stress σ_{max} vs. γ_{max} are shown for cyclic strain (CS) (circle and square denote $N = 4000$ and 32000 respectively, with filled and open symbols corresponding to glasses from $T = 0.466$ and $T = 1$). The vertical line at $\gamma_{max} = 0.08$ indicates the sharp yielding transition seen. (c) Energy vs. strain in the steady states, displaying a bifurcation in the strain corresponding to minima in energy at the yielding transition between $\gamma_{max} = 0.07$ and 0.08 . (d) Strain values corresponding to energy minima ($\gamma_{U_{min}}$) and zero stress (γ_{σ_0}) are shown as open and filled symbols respectively, vs. the number of cycles for different γ_{max} . For $\gamma_{max} = 0.08$ an initial relaxation towards zero is reversed as the system evolves to a yielded steady state with finite $\gamma_{U_{min}}$ and γ_{σ_0} . (e) $\gamma_{U_{min}}$ and γ_{σ_0} as functions of strain amplitude γ_{max} , displaying a transition beyond $\gamma_{max} = 0.07$. (f) Asymptotic energy per particle at $\gamma = 0$ vs. strain amplitude γ_{max} . Energies decrease with γ_{max} till the yield strain is reached, after which they increase with γ_{max} .

sizes. This is in contrast with the case of uniform shear, wherein both energy drops and avalanche sizes show a gradual, and strongly sample dependent, variation with strain (see Supporting Information).

Percolation.- Finally, we analyse the spatial structure of the avalanches briefly, by studying (i) the percolation,

and (ii) fractal dimension, of the avalanches. Below γ_y , none of the avalanches percolate, whereas above, a finite fraction does so. Figure 4(a) shows the weight of the spanning cluster P_∞ , and percolation probability PP averaged over bins in “probability” P , obtained from the fraction of displaced particles, (see Methods) for differ-

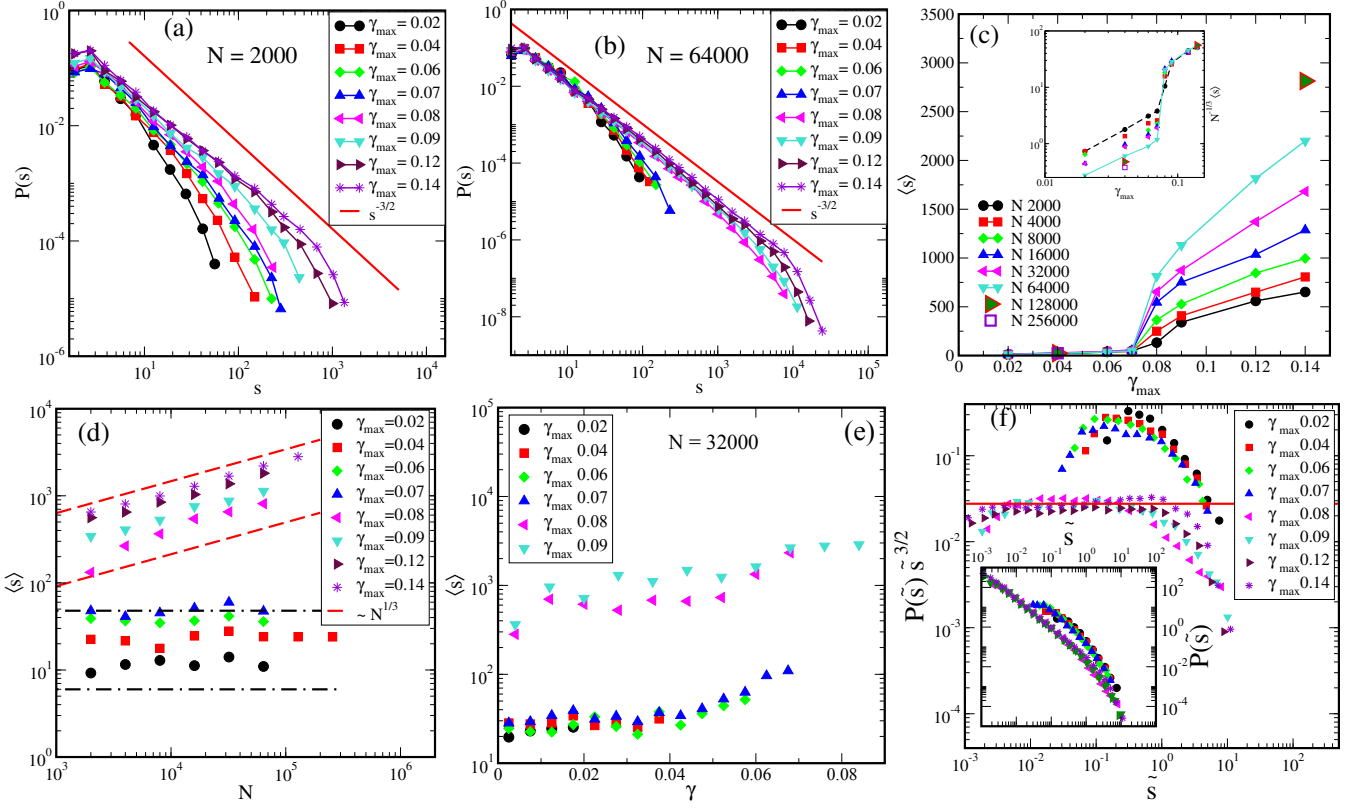


FIG. 2. Statistics of avalanches as a function of strain amplitude γ_{max} and system size N : (a) Cluster size distributions for $N = 2000$ displaying a power law with a cutoff that grows with γ_{max} but does not indicate sharp changes at yielding. (b) Cluster size distribution for $N = 64000$ displaying a sharp increase in the cutoff size across the yielding transition. The line in both panels corresponds to a power law with exponent $-3/2$. (c) Mean cluster size vs. γ_{max} showing a qualitative change across the yielding transition, with strong system size dependence above γ_y . The inset shows the mean cluster size scaled with $N^{1/3}$, which describes well the size dependence above γ_y . (d) Mean cluster size vs. system size N shows no significant size dependence for $\gamma_{max} < \gamma_y$ but a clear $N^{1/3}$ dependence above. A crossover in behaviour is seen for $\gamma_{max} = 0.08$. Lines, with N^0 (constant) and $N^{1/3}$ dependence, are guides to the eye. (e) Mean cluster sizes for bins in strain γ for different γ_{max} for $N = 32000$. Mean cluster size does not depend on γ_{max} , and depends only mildly on strain γ , for two distinct sets, below and above yield strain γ_y . (f) Scaled cluster size ($\tilde{s} = s / \langle s \rangle$) distributions exhibit data collapse separately for $\gamma_{max} < \gamma_y$ and $\gamma_{max} > \gamma_y$ (inset). Distributions for $\gamma_{max} < \gamma_y$ do not display a power law regime, whereas $\gamma_{max} > \gamma_y$ do, over about two decades in \tilde{s} , as highlighted in a plot of $P(\tilde{s})\tilde{s}^{3/2}$ vs. \tilde{s} . Data shown are for $T = 1$, and averages are over the full cycle, except for (e) which are averaged over the first quadrant.

ent system sizes for $\gamma_{max} = 0.08$, indicating a percolation transition at $P \gtrsim 0.05$. However, the threshold is system size dependent, and thus merits further investigation. In Fig 4 (b), P_∞ and PP averaged over all considered events are shown as a function of γ_{max} . The percolation probability does not become 1, a result of considering all the drop events. To address this artefact we analyse the cumulative set of all particles displaced in any of the events. The P_∞ and PP values shown in Figure 4 (c) indicate that above γ_y , this cumulative set always percolates and the weight P_∞ is comparable for different system sizes. However, P_∞ at the smallest γ_{max} above γ_y appears to increase with system size, suggesting a discontinuous change across γ_y . The variation of P with γ_{max} in either method also shows an apparently discontinuous behaviour across γ_y (see Supporting Infor-

mation).

Fractal Dimension.— We compute the fractal dimension of the spanning clusters using the box counting method (see Methods). Figure 4 (d) shows a log-log plot of the occupied boxes vs. magnification r (the largest r corresponds to the smallest box size, of $1.1\sigma_{AA}$) for $\gamma_{max} = 0.08$, $N = 32000$. We find a fractal dimension of $d_f = 2.05$, close to 2, which appears consistent with the possibility that yield events are quasi-two dimensional. However, based on the system size dependence of the mean cluster size, the fractal dimension deduced is $d_f \sim 1$ [13], which is at odds with the result here, and requires further investigation for it to be properly understood.

The results that we have discussed demonstrate that a sharp yielding transition is revealed through oscilla-

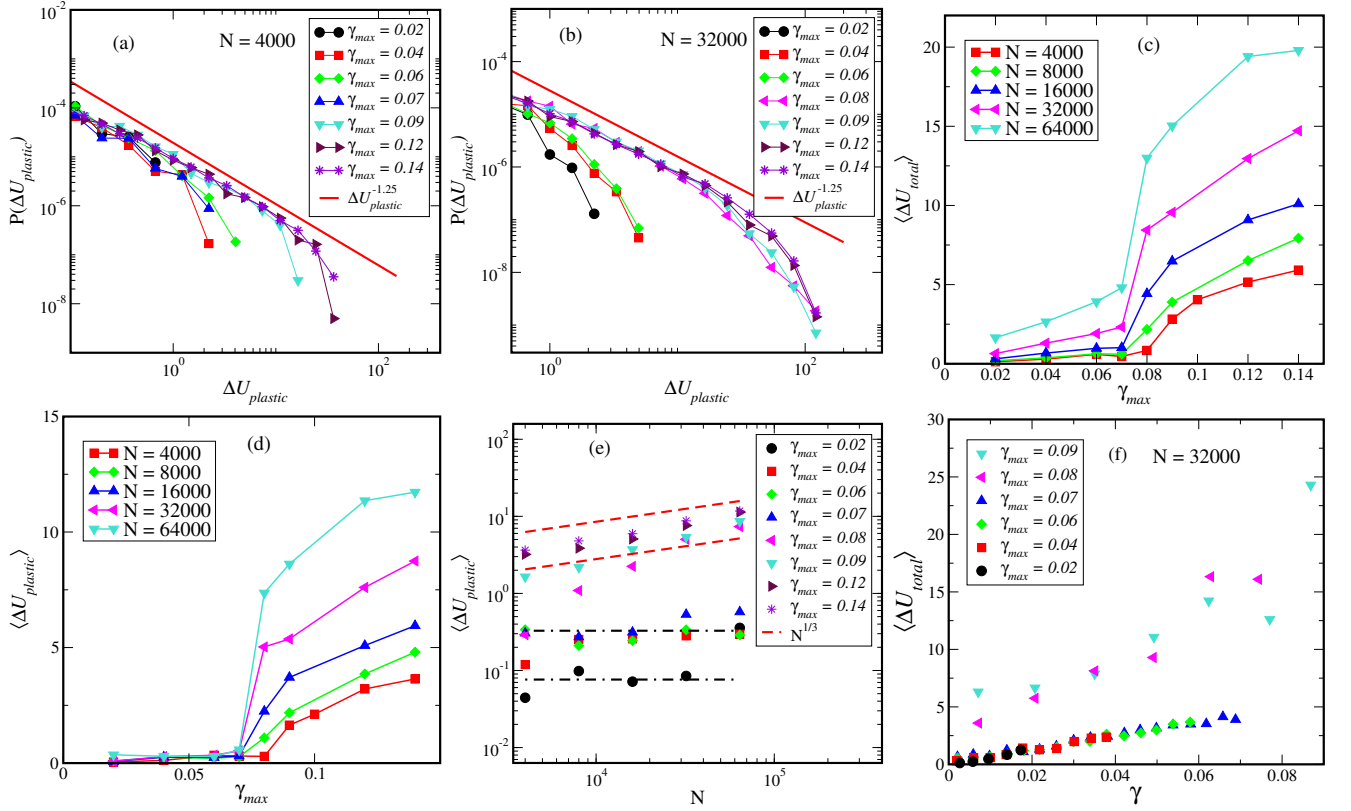


FIG. 3. Statistics of energy drops as a function of strain amplitude γ_{max} and system size N : Distributions of energy drops (a) for $N = 4000$ show no clear separation of $\gamma_{max} < \gamma_y$ and $\gamma_{max} > \gamma_y$ whereas (b) for $N = 32000$ a clear separation is visible. In both cases, a power law regime is apparent, with exponent ~ 1.25 . (c) Mean energy drops vs. γ_{max} , indicating a sharp change at γ_y . (d) Mean energy drops considering only plastic regions show no system size dependence below γ_y . (e) Mean energy drop (plastic component) vs. system size N shows no significant size dependence for $\gamma_{max} > \gamma_y$ but a clear $N^{1/3}$ dependence above. A crossover in behaviour is seen for $\gamma_{max} = 0.08$. Lines, with N^0 (constant) and $N^{1/3}$ dependence, are guides to the eye. (f) Mean energy drops (total) for bins in strain γ for different γ_{max} for $N = 32000$, $T = 1$ showing no dependence on γ_{max} , and only a mild dependence on strain γ , for two distinct sets, below and above yield strain γ_y . Data shown are for $T = 1$, and averages are over the first quadrant.

tory deformation of model glasses. The character of the avalanches is qualitatively different across the transition, being localised below the transition, and becoming extended above. Contrary to theoretical expectations for uniform deformation, the mean size of the avalanches does not diverge upon approaching the yielding transition, and prompts theoretical investigation, including development of suitable elasto-plastic models, of yielding under oscillatory deformation[29]. A signature of yielding is instead revealed by the progressive sluggishness of annealing behaviour as the transition is approached. Both the avalanche statistics and percolation characteristics suggest a discontinuous yielding transition, which may be consistent with the suggestion that yielding is a first order transition [14]. Finally, our results reveal systematic, non-trivial annealing behaviour of the glasses near the yielding transition, which we believe are of relevance to thermomechanical processing of metallic glasses. In particular, processing near the yielding transition, both above and below, may lead to significant change of prop-

erties, which may be utilised according to specific design goals.

Methods.— The model system we study is the Kob-Andersen binary (80:20) mixtures of Lennard Jones particles. The interaction potential is truncated at a cutoff distance of $r_{c\alpha\beta} = 2.5\sigma_{\alpha\beta}$ such that both the potential and the force smoothly go to zero as given by

$$V_{\alpha\beta}(r) = 4\epsilon_{\alpha\beta} \left[\left(\frac{\sigma_{\alpha\beta}}{r} \right)^{12} - \left(\frac{\sigma_{\alpha\beta}}{r} \right)^6 \right] + 4\epsilon_{\alpha\beta} \left[c_{0\alpha\beta} + c_{2\alpha\beta} \left(\frac{r}{\sigma_{\alpha\beta}} \right)^2 \right], r_{\alpha\beta} < r_{c\alpha\beta}(1)$$

where $\alpha, \beta \in \{A, B\}$ and the parameters $\epsilon_{AB}/\epsilon_{AA} = 1.5$, $\epsilon_{BB}/\epsilon_{AA} = 0.5$, $\sigma_{AB}/\sigma_{AA} = 0.80$, $\sigma_{BB}/\sigma_{AA} = 0.88$. Energy and length are in the units of ϵ_{AA} and σ_{AA} respectively, and likewise, reduced units are used for other quantities. The correction terms $c_{0\alpha\beta}, c_{2\alpha\beta}$ are evaluated with the conditions that the potential and its derivative at $r_{c\alpha\beta}$ must vanish at the cutoff.

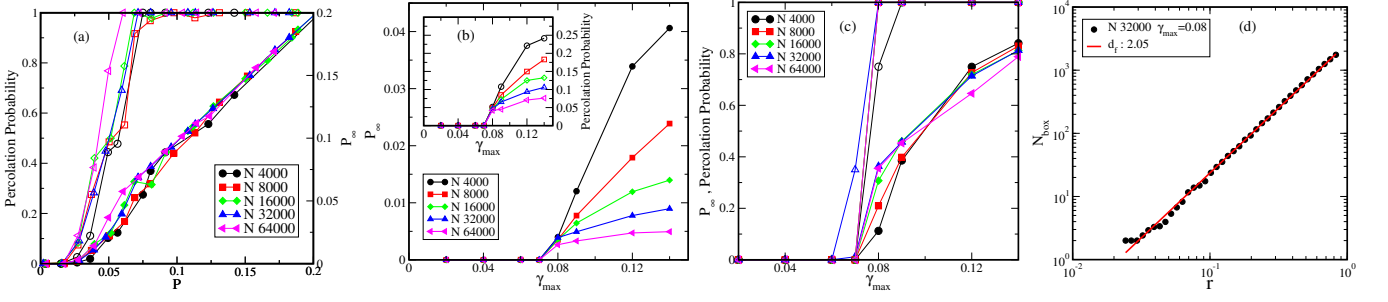


FIG. 4. Percolation of avalanches and fractal dimension of percolating clusters: **(a)** Percolation probability and weight of the spanning cluster P_∞ shown as open and filled symbols respectively against the occupation number P for different system sizes, considering all events, for $\gamma_{max} = 0.08$. A percolation transition takes place for $P \simeq 0.05$ although the threshold is system size dependent. **(b)** Percolation probability (inset) and P_∞ averaged over all events, *vs.* γ_{max} . **(c)** Percolation probability and P_∞ for the cumulative set of particles rearranging over a cycle, shown as open and filled symbols respectively *vs.* γ_{max} , indicating a percolation transition at the yielding strain γ_y . P_∞ just above the transition increases with system size. **(d)** Fractal dimension estimation from box counting. A log-log plot of the number of occupied boxes (N_{box}) is shown *vs.* the magnification r . The slope results in an estimated fractal dimension $d_f = 2.05$. Data shown are for $T = 1$, and averages are over the first quadrant.

The initial liquid samples are equilibrated at two temperatures, $T = 0.466$ and $T = 1$ using the Nosé Hoover thermostat, at reduced density $\rho = 1.2$. Independent samples are generated for each temperature and system size by further evolving the equilibrated liquid configurations by performing the molecular dynamics simulations of constant energy, which are separated by the structural relaxation time (τ_α) obtained from the self intermediate scattering function ($F_s(k, t)$). For the uniform shearing data, we have at least 100 samples for all the system sizes. The avalanche data shown for cyclic shearing are for at least 20 samples for $N \leq 32000$, and 10 samples for larger systems. All the simulations are carried out using LAMMPS [30].

Shear deformation of the model amorphous solids is done employing athermal-quasi static (AQS) simulations which consist of two steps. An affine transformation of coordinates $x' = x + d\gamma \times z$; $y' = y$; $z' = z$ is imposed, subsequently followed by an energy minimization using the conjugate-gradient method with Lees-Edwards periodic boundary conditions. Strain steps of $d\gamma = 2 \times 10^{-4}$ are used throughout, except for $N = 256000$ for which $d\gamma = 5 \times 10^{-4}$. Initial configurations are the inherent structures (local energy minima) of equilibrated liquid samples. Potential energy and mean square displacements are computed at $\gamma = 0$ as functions of cycles to ascertain that steady states are reached, wherein the coordinates of particles, and properties such as the potential energy U and shear stress σ_{xz} remain (below yield strain) unchanged at the end of each cycle, or (above yield strain) become statistically unchanged upon straining further, and exhibit diffusive motion as a function of the number of cycles. Steady states for strain amplitudes of $\gamma_{max} = 0.02, 0.04, 0.06, 0.07, 0.08, 0.09, 0.12, 0.14$ are studied for system sizes $N = 2000, 4000, 8000, 16000, 32000$ and 64000. To further probe finite size effects, we have considered amplitude below the yield transition at $\gamma_{max} = 0.04$

for $N = 128000$ and 256000, and $\gamma_{max} = 0.14$ for $N = 128000$.

In the steady state, we compute the potential energy per particle and stress for each strain step. Plastic events result in discontinuous energy and stress drops. A parameter $\kappa = \frac{\delta U}{N d\gamma^2}$ [27] exceeding a value of 100 is used to identify plastic events, where δU is the change in energy during minimisation after a strain step. Avalanche sizes based on the magnitude of energy drops and the cluster sizes of “active” particles (that undergo plastic displacements) are both computed. Particles are considered active if they are displaced by more than $0.1\sigma_{AA}$. The choice of this cutoff is based on considering the distribution of single particle displacements δr , which are expected to vary as a power law $P(\delta r) \sim \delta r^{-5/2}$ for elastic displacements around a plastic core, but display an exponential tail corresponding to plastic rearrangements (see, *e. g.*, [23]). The separation is clear cut only for small γ_{max} , and we choose the smallest cutoff value (observed for $\gamma_{max} = 0.02$) so that plastic rearrangements at all γ_{max} are considered. In performing cluster analysis, two active particles are considered to belong to the same cluster if they are separated by less than $1.4\sigma_{AA}$ (first coordination shell). The normalised histogram of cluster sizes $P(s)$ is obtained from statistics for all the events. The mean cluster size is computed from the distributions as $\langle s \rangle = \frac{\sum_s s^2 P(s)}{\sum_s s P(s)}$ (see Supporting Information).

For the percolation analysis, we consider all the plastic events in the first quadrant of the cycle (γ from 0 to γ_{max}), and compute the “probability” P from the fraction of particles that undergo plastic displacement, and the weight of the spanning cluster P_∞ , from the fraction of particles that belong to the spanning cluster ($P_\infty = 0$ if there is no spanning cluster). The percolation probability $PP = 1$ if a spanning cluster is present and 0 otherwise.

To obtain the fractal dimension of percolating clusters, we employ the method of box counting. The simulation

volume is divided into boxes of a specified mesh size, and the number of boxes that contain a part of the cluster, N_{box} , is counted. This is repeated for a series of mesh sizes, and the fractal dimension is obtained as the slope $d_f = \frac{\log(N_{box})}{\log r}$ where r is the inverse of mesh size.

ACKNOWLEDGMENTS

We wish to thank J. L. Barrat, P. Chaudhuri, M. Falk, G. Foffi, A. L. Greer, J. Horbach, I. Procaccia, M. Rob-

bins, A. Rosso and M. Wyart for useful discussions. We wish to specially thank H. A. Vinutha for discussions and help regarding computations reported here. We gratefully acknowledge TUE-CMS and SSL, JNCASR, Bengaluru for computational resources and support.

-
- [1] M. L. Falk and J. Langer, *Annu. Rev. Condens. Matter Phys.* **2**, 353 (2011).
 - [2] J. L. Barrat and A. Lemaître, in *Dynamical heterogeneities in glasses, colloids, and granular media*, edited by L. Berthier, G. Biroli, J. P. Bouchaud, L. Cipelletti, and W. v. Saarloos (Oxford Science Publications, Oxford, 2011) Chap. 8, pp. 264–297.
 - [3] C. E. Maloney and A. Lemaître, *Phys. Rev. E* **74**, 016118 (2006).
 - [4] K. A. Dahmen, Y. Ben-Zion, and J. T. Uhl, *Phys. Rev. Lett.* **102**, 175501 (2009).
 - [5] S. Karmakar, E. Lerner, and I. Procaccia, *Phys. Rev. E* **82**, 055103 (2010).
 - [6] R. Dasgupta, H. G. E. Hentschel, and I. Procaccia, *Phys. Rev. Lett.* **109**, 255502 (2012).
 - [7] N. C. Keim and P. E. Arratia, *Soft Matter* **9**, 6222 (2013).
 - [8] J. Lin, E. Lerner, A. Rosso, and M. Wyart, *Proceedings of the National Academy of Sciences* **111**, 14382 (2014).
 - [9] D. J. P. E. D. Knowlton and L. Cipelletti, *Soft Matter* **10**, 6931 (2014).
 - [10] K. Hima Nagamanasa, S. Gokhale, A. K. Sood, and R. Ganapathy, *Phys. Rev. E* **89**, 062308 (2014).
 - [11] G. P. Shrivastav, P. Chaudhuri, and J. Horbach, *Phys. Rev. E* **94**, 042605 (2016).
 - [12] I. Regev, J. Weber, C. Reichhardt, K. A. Dahmen, and T. Lookman, *Nature communications* **6** (2015).
 - [13] C. Liu, E. E. Ferrero, F. Puosi, J.-L. Barrat, and K. Martens, *Phys. Rev. Lett.* **116**, 065501 (2016).
 - [14] P. K. Jaiswal, I. Procaccia, C. Rainone, and M. Singh, *Phys. Rev. Lett.* **116**, 085501 (2016).
 - [15] P. Hébraud and F. Lequeux, *Phys. Rev. Lett.* **81**, 2934 (1998).
 - [16] Y. H. Sun, A. Concustell, and A. L. Greer, *Nat. Rev. Mater.* **1** (2016), doi:10.1038/natrevmats.2016.39.
 - [17] A. Argon, *Acta Metall.* **27**, 47 (1979).
 - [18] G. Picard, A. Ajdari, F. Lequeux, and L. Bocquet, *The European Physical Journal E* **15**, 371 (2004).
 - [19] M. Talamali, V. Petäjä, D. Vandembroucq, and S. Roux, *Comptes Rendus Mécanique* **340**, 275 (2012).
 - [20] S. Ganguli, J. Horbach, P. Sollich, S. Karmakar, and S. Sengupta, *arXiv preprint arXiv:1603.05092* (2016).
 - [21] K. M. Salerno and M. O. Robbins, *Phys. Rev. E* **88**, 062206 (2013).
 - [22] J. P. Sethna, K. A. Dahmen, and C. R. Myers, *Nature* **410**, 242 (2001).
 - [23] D. Fiocco, G. Foffi, and S. Sastry, *Phys. Rev. E* **88**, 020301 (2013).
 - [24] N. V. Priezjev, *Phys. Rev. E Stat. Nonlin. Soft Matter Phys.* **87**, 052302 (2013).
 - [25] I. Regev, T. Lookman, and C. Reichhardt, *Phys. Rev. E Stat. Nonlin. Soft Matter Phys.* **88**, 062401 (2013).
 - [26] C. Deng and C. A. Schuh, *Appl. Phys. Lett.* **100**, 251909 (2012).
 - [27] E. Lerner and I. Procaccia, *Phys. Rev. E* **79**, 066109 (2009).
 - [28] D. Fiocco, G. Foffi, and S. Sastry, *Phys. Rev. Lett.* **112**, 025702 (2014).
 - [29] N. Perchikov and E. Bouchbinder, *Phys. Rev. E* **89**, 062307 (2014).
 - [30] S. Plimpton, *J. Comput. Phys.* **117**, 1 (1995).

The yielding transition in amorphous solids under oscillatory shear deformation (Supplementary Information)

Premkumar Leishangthem, Anshul D. S. Parmar and
Srikanth Sastry

Here we provide additional information regarding the following aspects of analysis of model glasses subjected to oscillatory deformation: (i) Number of cycles required to reach the steady state, (ii) Evolution of energy with cycles, (iii) Identification of particles undergoing plastic displacements, (iv) Avalanche distributions at different strain for different strain amplitudes (v) Energy drops and avalanche sizes for uniform shear, and (vi) Probability of plastic displacement as a function of strain amplitude.

I. NUMBER OF CYCLES REQUIRED TO REACH THE STEADY STATE

We analyse the potential energy $U(\gamma = 0)$ *vs.* the number of cycles n to probe the approach to the steady state, and denote by n^* the indicative number of cycles needed to reach the steady state, and is obtained as a decay constant by fitting the cycle dependence of energies to the form $U(n) = U_\infty + \Delta U_0 \exp[-(n/n^*)^\beta]$. These fits are shown in Fig. S1 (a), (b) for $\gamma_{max} < \gamma_y$ (for the $T = 1$ cases) and $\gamma_{max} > \gamma_y$ (for both $T = 1$ and $T = 0.466$) respectively. Fig. S1(c) shows that n^* grows strongly on approaching the yield value of γ_{max} between 0.07 and 0.08. The fit lines are guides to the eye.

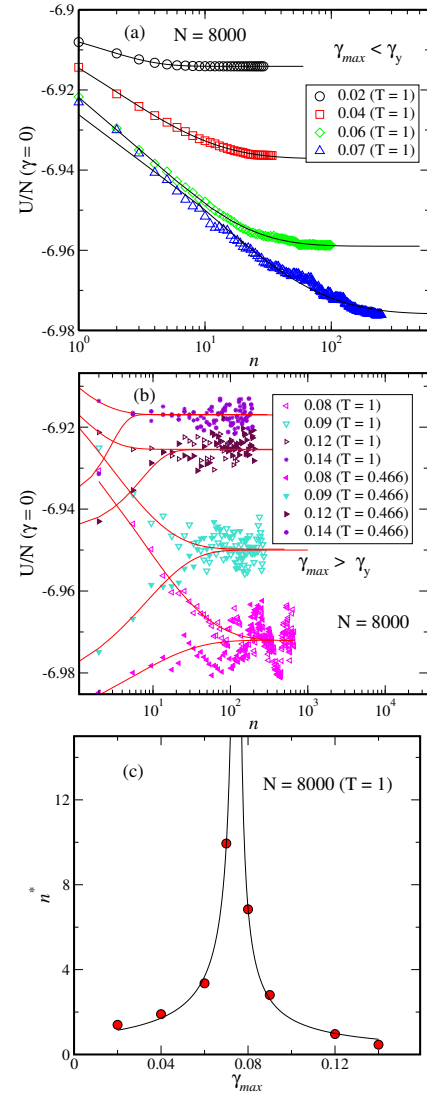


FIG. S1. Energy *vs.* cycle for different strain amplitudes (a) below and (b) above the transition. (c) The decay constant n^* to reach the steady state.

II. EVOLUTION OF ENERGY WITH CYCLES

We present here the potential energy at each strain step over the cycles of deformation for $\gamma_{max} = 0.06$ and 0.12 in Fig. S2. The strain at $U = U_{min}$ and $\sigma_{xz} = 0$ are represented by $\gamma_{U_{min}}$ and γ_{σ_0} . To test if the location of the energy minima coincide with the strain at zero stress, *i. e.* if $\gamma_{U_{min}} = \gamma_{\sigma_0}$, we plot the energy and the stress loops in Fig. S3 for $\gamma_{max} = 0.14$ of $N = 64000$ ($T=1$). Though their values are close, we find $\gamma_{U_{min}} \neq \gamma_{\sigma_0}$ (for $\gamma_{max} > \gamma_y$).

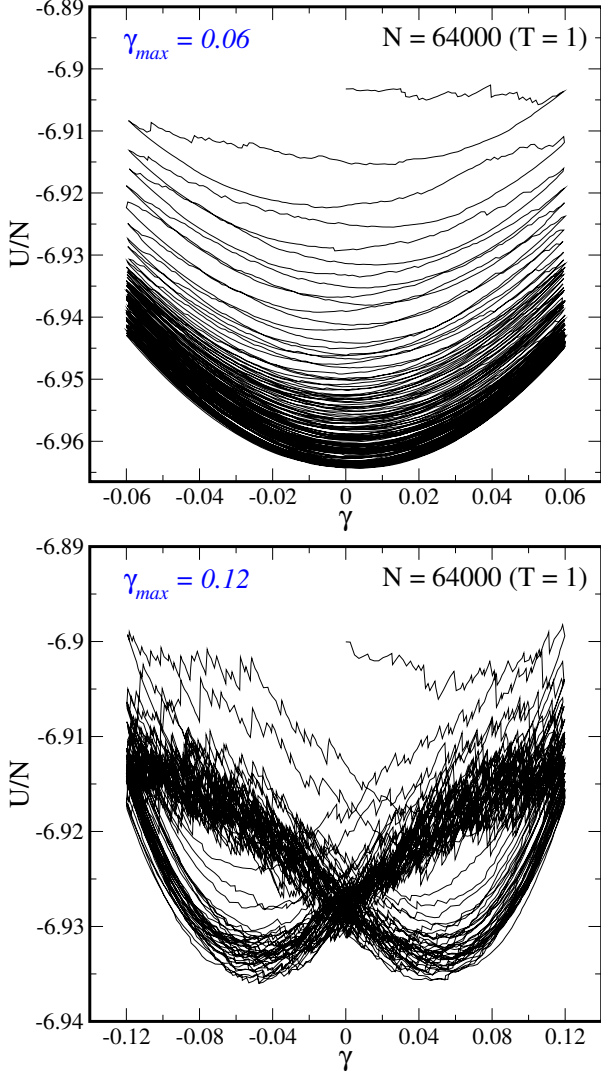


FIG. S2. Energy *vs.* strain over cycles starting with the undeformed glass, showing (for $\gamma_{max} = 0.06$) the approach to a single minimum at $\gamma = 0$, and bifurcation into two minima (for $\gamma_{max} = 0.12$) at finite strain.

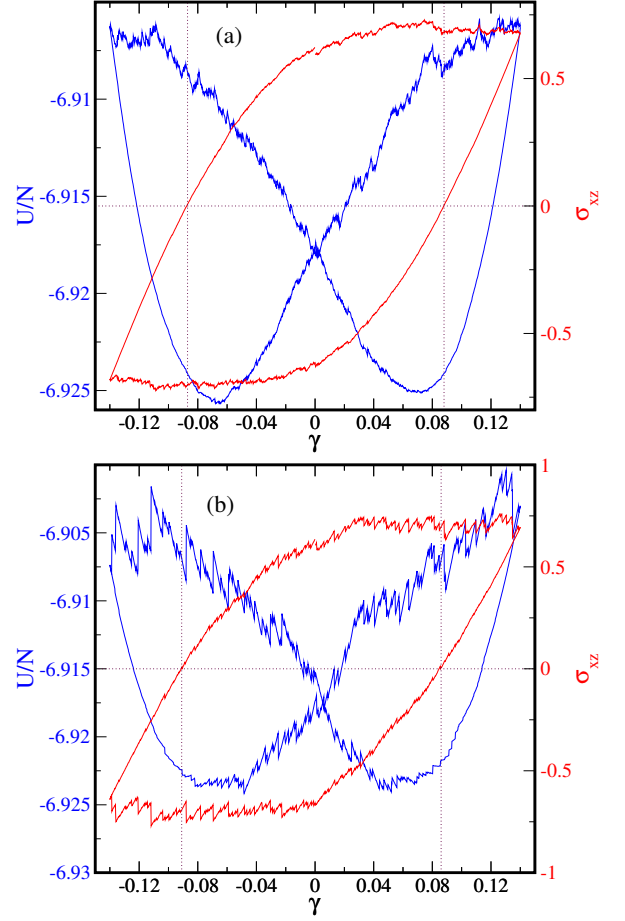


FIG. S3. Stress *vs.* strain (red lines) and energy *vs.* strain (blue lines) are shown, along with with dotted lines as guides to the eye, to locate $\sigma_{xz} = 0$. Data shown are (a) averaged over 10 cycles and (b) for a single cycle, in the steady state.

III. IDENTIFICATION OF PARTICLES UNDERGOING PLASTIC DISPLACEMENTS

Here we describe how particles that are labeled “active”, that undergo plastic deformation during an energy drop, are identified, based on previous work [see, *e. g.* D. Fiocco, G. Foffi and S. Sastry, Phys. Rev. Lett. 025702 (2014); T. B. Schroder, S. Sastry, J. C. Dyre, and S. C. Glotzer, J. Chem. Phys. 112, 9834 (2000)]. In the presence of a plastic rearrangement, it is found that the distribution of single particle displacements $p(\delta r)$ displays an exponential tail, corresponding to plastic displacements, and a power law distribution at smaller values with an exponent of $-5/2$ which may be deduced from assuming that the rest of the system undergoes an elastic deformation owing to the stresses created by the plastic deformation. As seen in Fig. S4, such an expectation is clearly satisfied at low strain amplitudes γ_{max} , but (a) the location of the crossover depends on the strain amplitude, and (b) the distinction becomes less clear at large strain amplitudes. We wish to include all particles that take

part in plastic deformation, but to exclude those undergoing elastic displacements. As a conservative choice of cutoff, we use the cutoff that is clear and applicable for the case of $\gamma_{max} = 0.02$, namely $\delta r = 0.1$.

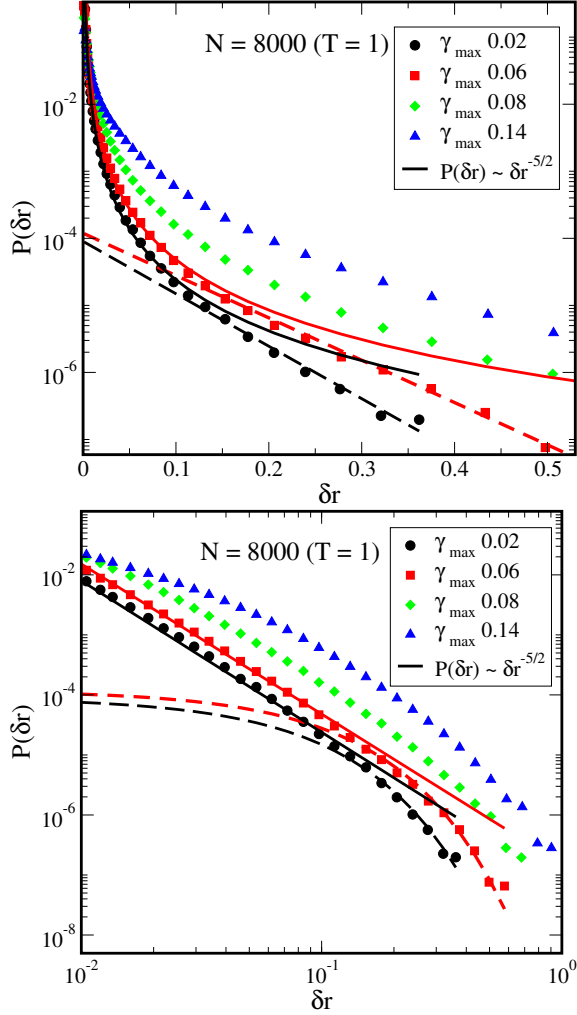


FIG. S4. Distributions of the particle displacements at the plastic events shown in semi-log and log-log scales for various strain amplitudes.

IV. AVALANCHE DISTRIBUTIONS AT DIFFERENT STRAIN FOR DIFFERENT STRAIN AMPLITUDES

We show here the distribution of avalanche sizes that result when specific bins in the strain γ are considered, for different amplitudes γ_{max} , with results averaged over the first quadrant of cycles of strain. Fig. S5 shows the distribution of avalanche sizes in the strain window of (a) 0 to 0.02, and (b) 0.04 to 0.06, for different values of γ_{max} for which we sample the strain window in the course of a full cycle. We note that in both bases, the distributions fall into two categories, one with $\gamma < \gamma_y$ and

the other with $\gamma > \gamma_y$. In each category, the distributions are largely independent of the value of γ_{max} , but the distributions for the two categories are distinct.

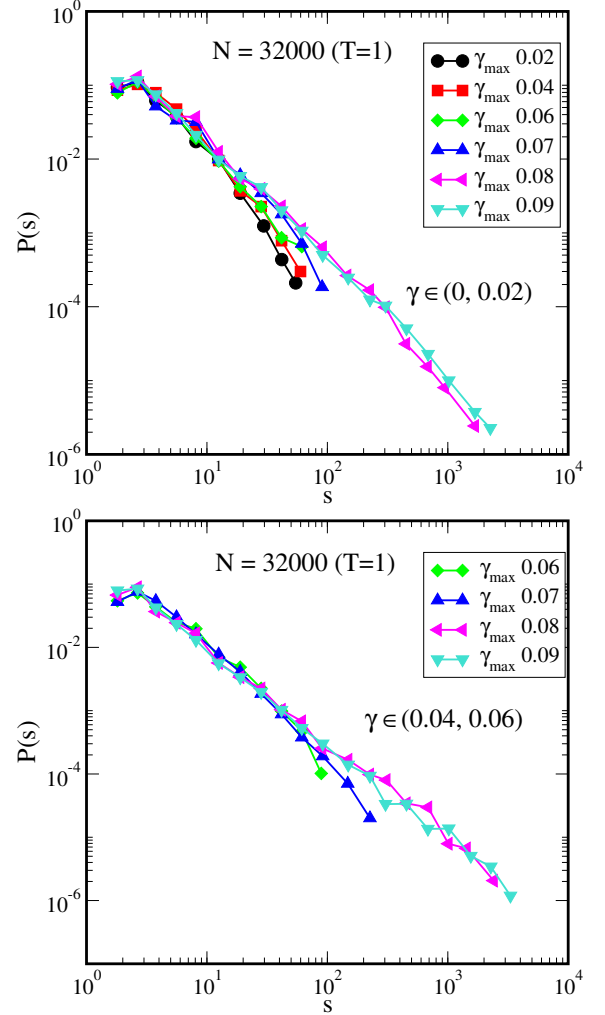


FIG. S5. Distributions of avalanche sizes within specified windows of strain [(left panel) 0 to 0.02, and (right panel) 0.04 to 0.06] for different strain amplitudes.

V. ENERGY DROPS AND AVALANCHE SIZES FOR UNIFORM SHEAR

In Fig. S6 we present the mean energy drop for uniform strain, for $T = 1$ and $T = 0.466$, for a range of system sizes for a range of system sizes. We see that the mean energy drops for the two temperatures are significantly different, but in each case show similar trends in their system size dependence. In Fig. S7, we compare, for $N = 4000$, the mean size of avalanches and the mean energy drop, for $T = 1$ and $T = 0.466$. The behaviour for the two cases is very different at strains below the yield strain, thus making it difficult to provide a general characterisation of the avalanches below the yield strain

identified by oscillatory deformation. Further, we note that for $T = 1$, the energy drops and avalanche sizes below the yield strain remain high and comparable to values above yield strain. Fig. S8 shows the distributions of energy drops for two strain intervals (one below, $\{0, 0.02\}$, and one above, $\{0.2, 0.5\}$, the yield strain). For $T = 1$, the two distributions do not differ, whereas for $T = 0.466$, they are widely separated. The avalanche size distributions shown in Fig. S9 show the same pattern.

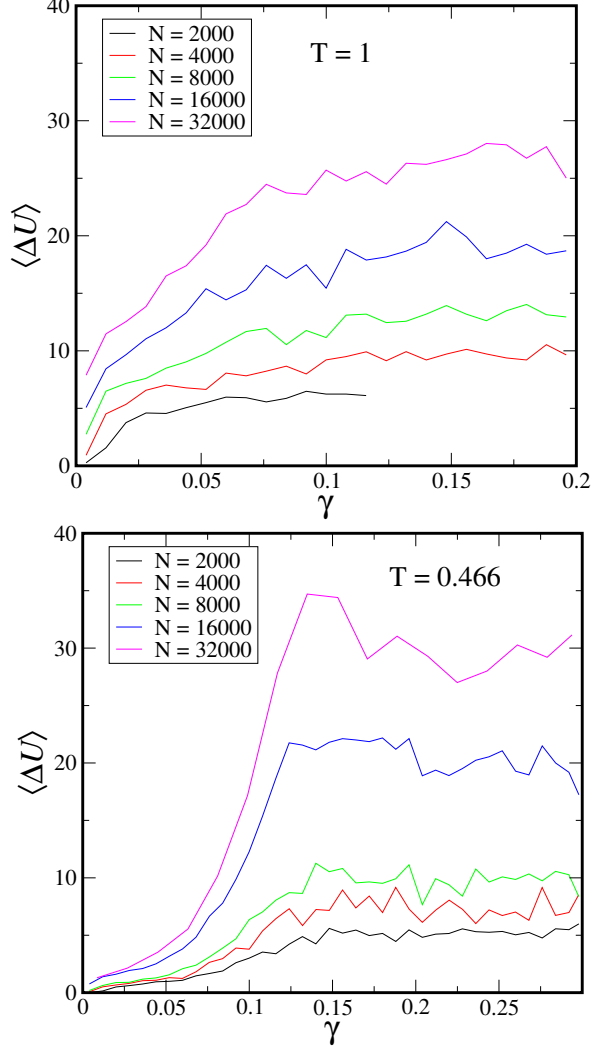


FIG. S6. Mean energy drops *vs.* strain for various system sizes for uniform strain.

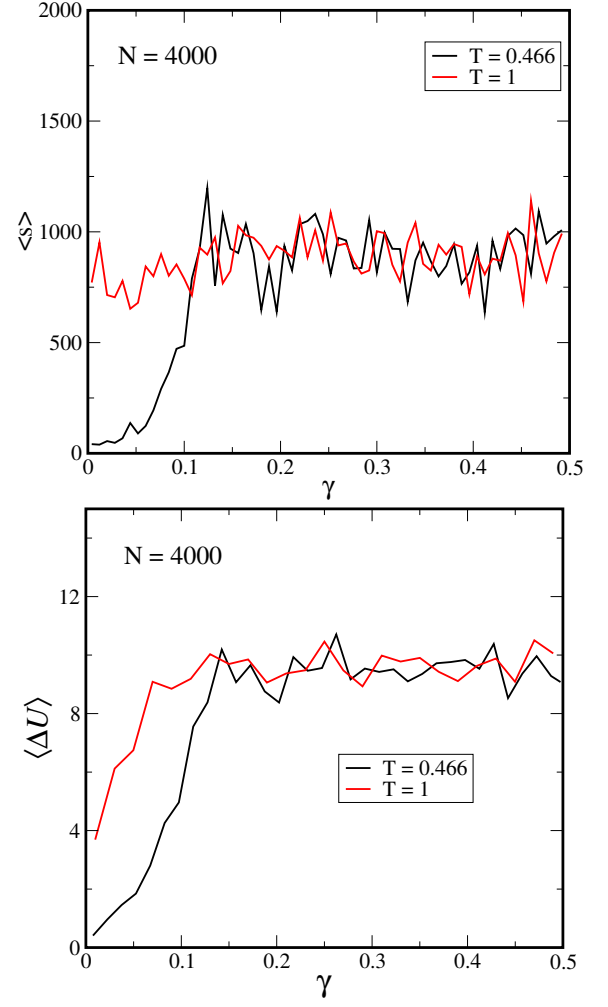


FIG. S7. Mean avalanche size and mean energy drops *vs.* strain for $T = 1$ and $T = 0.466$, $N = 4000$.

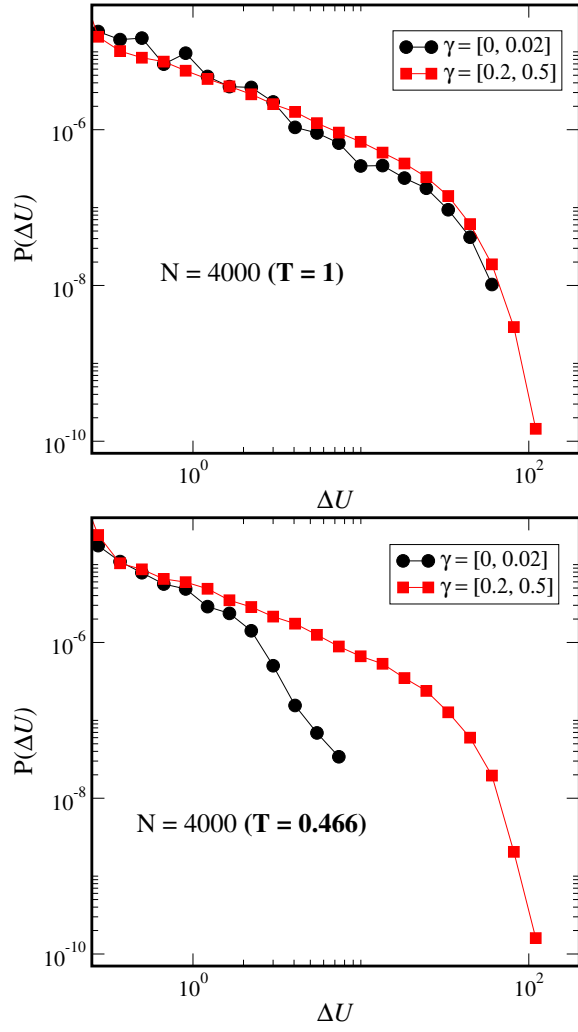


FIG. S8. Distributions of energy drops for two windows of strain, below and above the yielding transition, shown for $T = 1$ and $T = 0.466$.

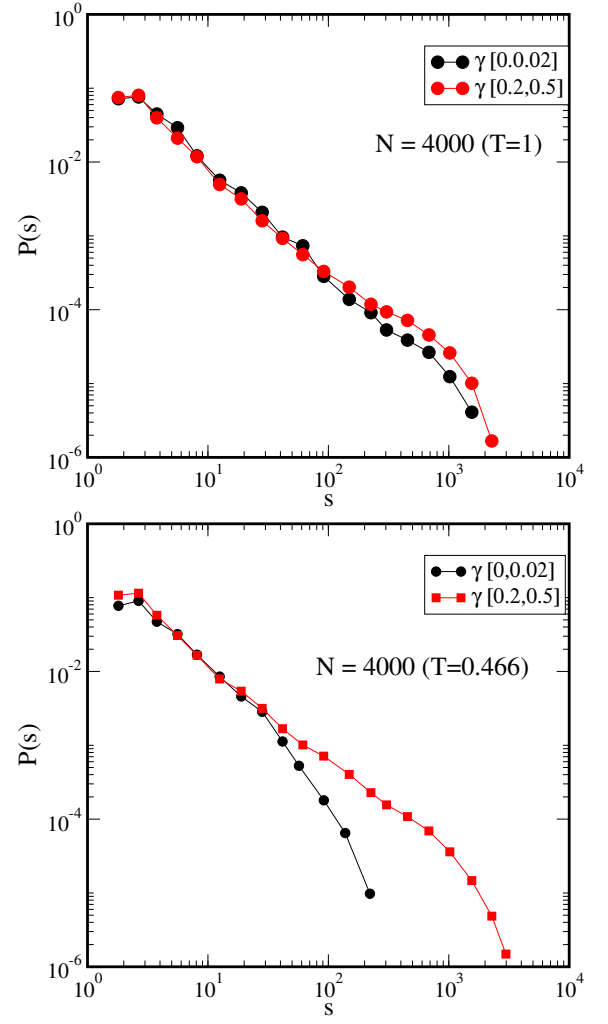


FIG. S9. Distributions of avalanche sizes for two windows of strain, below and above the yielding transition, shown for $T = 1$ and $T = 0.466$.

VI. PROBABILITY OF PLASTIC DISPLACEMENT AS A FUNCTION OF STRAIN AMPLITUDE

We show in Fig. S10 the average fraction of active particles, or probability P , (ratio of the number of active particles and the total number of particles) for different system sizes, as a function of strain amplitude γ_{max} . The averages are performed over the first quadrant of the strain cycles. In Fig. S10(a) the probability P is for individual drop events, averaged over all events, whereas in Fig. S10 (b) P is obtained for each cycle by accumulating all particles that are active in any of the drop events that occur, and the averaging is done over all cycles. In both cases, P changes sharply across the yield strain, but with different system size dependence.

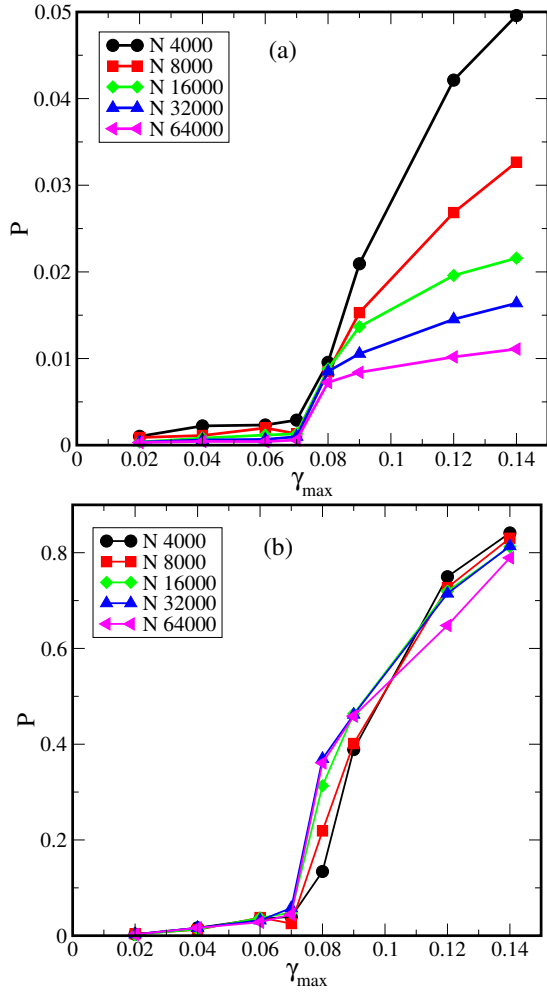


FIG. S10. Fraction of active particles P *vs.* strain amplitude γ_{max} , for different system sizes, (a) for individual drop events, and (b) accumulated over the first quadrant of cycles of strain.